optica

Single-pixel optical camera for video rate ultrasonic imaging

Nam Huynh,[1] Edward Zhang,[1] Marta Betcke,[2] Simon Arridge,[2] Paul Beard,[1] and Ben Cox[1,*]

[1]Department of Medical Physics and Biomedical Engineering, University College London, WC1E 6BT, UK
[2]Department of Computer Science, University College London, WC1E 6BT, UK
*Corresponding author: b.cox@ucl.ac.uk

Received 1 September 2015; revised 28 October 2015; accepted 16 November 2015 (Doc. ID 247610); published 6 January 2016

A coherent-light single-pixel camera was used to interrogate a Fabry–Perot polymer film ultrasound sensor, thereby serially encoding a time-varying 2D ultrasonic field onto a single optical channel. By facilitating compressive sensing, this device enabled video rate imaging of ultrasound fields. In experimental demonstrations, this compressed sensing capability was exploited to reduce motion blur and capture dynamic features in the data. This relatively simple and inexpensive proof-of-principle device offers a route to high pixel count, high frame rate, broadband 2D ultrasound field mapping.

OCIS codes: (120.2230) Fabry-Perot; (070.6120) Spatial light modulators; (110.7170) Ultrasound.

http://dx.doi.org/10.1364/OPTICA.3.000026

Recently, a class of optical imaging devices has begun to appear that are predicated on the idea that recording in time is cheap, but using photodetector arrays soon becomes expensive as the number of photodetecting elements grows. Examples include the Rice single-pixel camera [1], the STEAM camera [2], and the optofluidic microscope [3], all of which reduce the task of making highly resolved *spatial* measurements to that of recording sequentially in *time* using a single fixed detector. Here we present the first ultrasound field imaging device based on a similar optical time domain multiplexing principle.

Mapping broadband ultrasound fields in the tens of MHz range forms the basis of the high-resolution biomedical imaging modalities of photoacoustic tomography [4] and high-frequency ultrasound [5], as well as having direct relevance to nondestructive evaluation [6], materials characterization [7,8] high-frequency transducer calibration [9], metrology [10], and exposimetry [11]. Imaging broadband ultrasound fields at these frequencies in 2D using conventional piezoelectric or capacitive detector arrays (CMUTs) is extremely challenging because of the need for very high channel counts. This applies particularly at tens of MHz frequencies, where fulfilling the spatial Nyquist criterion requires a prohibitively complex and expensive 2D array typically comprising several thousand subwavelength elements and interelement spacings. Compressed sensing, or compressive sampling (CS), offers one possible route to reducing the number of measurements required to capture the information in the field, and for this reason it has found widespread success in optics [1] and magnetic resonance imaging [12], among other areas. However, CS requires a sequence of spatially integrated randomly sampled measurements of the acoustic field. While this could be achieved with an array of discrete piezoelectric detectors, it would require the same number of detectors as a fully sampled measurement, thus offering no advantage in terms of reducing cost and technical complexity. By contrast, if the acoustic field distribution can be encoded onto an optical field, then the latter can readily be spatially manipulated to meet the twin requirements of random sampling and spatial integration that a CS framework requires. In this Letter we demonstrate this concept by using a novel optical system that provides real-time 2D imaging of broadband ultrasound fields using just a single optical detector. It therefore provides the technological breakthrough required to overcome the main limitation of conventional fixed-element arrays.

In order to map spatial variations in acoustic pressure into spatial variations in optical intensity, a Fabry–Perot (FP) polymer thin-film etalon (Fig. 1) was illuminated by a wide-field collimated beam of coherent light from an external cavity laser. The beam reflected from the FP etalon was modulated by acoustically induced changes in the optical thickness of the etalon produced by an ultrasound transducer. The reflected beam, now carrying information about the acoustic field at the sensor surface, was subsequently sampled with a random spatial pattern using a digital micromirror device (DMD) before being spatially integrated by focusing onto a single photodiode, as shown in Fig. 2. FP etalons have previously been interrogated using single-point illumination [13–17] as well as multipixel cameras [11,18–21], but the former requires time-consuming sequential point scanning and the latter suffers from very low sampling rates. FP etalons [13] have been shown to exhibit bandwidths for ultrasonic detection from DC to many tens of MHz, and are capable of detecting with high sensitivity (low intrinsic noise) [13,22].

To describe how the sensor facilitates compressed sensing [23], we first introduce the following notation: the acoustic pressure on the FP etalon, which lies in the x–y plane, is denoted by $p(x, y, t)$ for time t, and the discretized pressure amplitude at the points on the etalon corresponding to the N individual DMD micromirrors

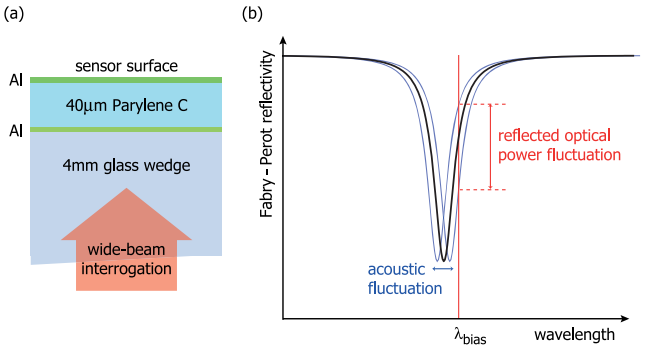

Fig. 1. Fabry–Perot polymer thin-film etalon ultrasound sensor. (a) Construction, see Supplement 1 (b) Optical reflectivity versus wavelength. By choosing the laser interrogation wavelength to be on the linear part of this interferometric transfer function, the deformation of the polymer layer caused by an acoustic wave passing through the sensor can be detected as a proportional change in the reflected optical power.

is given by $p_n^{(t)} = p(x_n, y_n, t)$, $n = 1, \ldots, N$. A snapshot of the entire sampled acoustic field at time t is then given by $\mathbf{p}^{(t)} = \{p_n^{(t)}, n = 1, \ldots, N\} \in \mathbb{R}^N$. Here, rather than recording $p_n^{(t)}$ at single points as might be done with a fixed-element detector array, integrals of the pattern-weighted field $\mathbf{p}^{(t)}$ are measured. In other words, the measurements are the set $\mathbf{w}^{(t)} = \{w_m^{(t)}, m = 1, \ldots, M\}$ given by the inner product $w_m^{(t)} = \langle \boldsymbol{\phi}_m, \mathbf{p}^{(t)} \rangle$, where the $\boldsymbol{\phi}_m$ are the measurement patterns (rows of the measurement matrix Φ). The measurements therefore consist of a set of time series, each corresponding to one of the patterns with which the acoustic pressure field was multiplied. There are two key notions in CS. The first is the assumption that the field can be represented *sparsely* in some—still to be specified—basis Ψ, $\mathbf{p}^{(t)} = \Psi \boldsymbol{a}^{(t)}$ (i.e., the field can be written as a sum of basis functions, $\boldsymbol{\psi}_q$, the columns of Ψ, weighted by the coefficients $a_q^{(t)}$, $q = 1, \ldots, Q$, such that $Q \ll N$). Second is the idea that the sparse coefficients $\boldsymbol{a}^{(t)}$ can be recovered from the data $\mathbf{w}^{(t)}$ measured using only $M \ll N$ measurement patterns $\boldsymbol{\phi}_m$ incoherent to Ψ. In other words, far fewer measurements are needed to obtain all the information in the data than when sampling at every point in the region of interest. Once sufficient data has been measured [23–25], the nonzero sparse coefficients $\boldsymbol{a}^{(t)}$ can be recovered using a nonlinear reconstruction approach, such as that described in Supplement 1. The success of CS depends on the incoherence of the basis Ψ and the measurement pattern matrix Φ, because it is not known in advance which of the coefficients is nonzero, and, hence, each measurement needs to capture some information about every coefficient. Often, not only are the sparse coefficients unknown in advance, but also the basis Ψ in which the data is sparse is unknown in advance. In such cases, it is necessary to use a measurement matrix Φ that is incoherent to a wide range of possible sparse bases. The scrambled Hadamard matrix was used here (see Supplement 1), as it has been shown to be close to optimal for general applications [26]. The two distinctive features of this single-pixel ultrasound field mapping camera system are the use of a patterned optical detection scheme to record ultrasound fields, and the use of CS to increase the frame rate and facilitate dynamic imaging. Several proof-of-principle experiments were performed to demonstrate these capabilities, using the setup shown schematically in Fig. 2 and further described in Supplement 1.

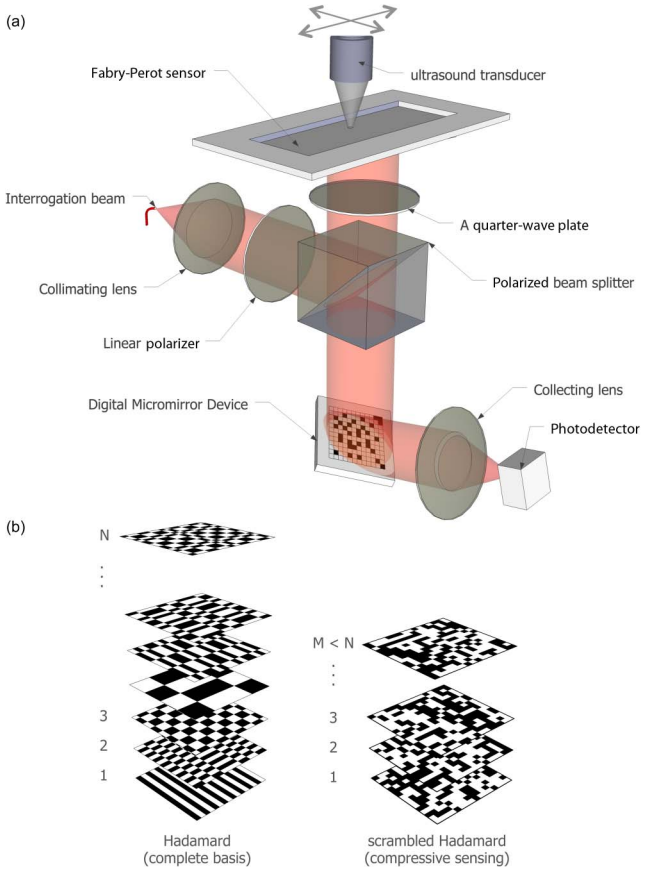

Fig. 2. Single-pixel camera for ultrasound field mapping. (a) Experimental arrangement and (b) Hadamard and scrambled Hadamard patterns used to sample the acoustic field on the sensor. See Supplement 1 for more details.

For all the examples, a dynamic ultrasound field was provided by a 15 MHz focused ultrasound transducer positioned about 20 mm above the FP sensor and focused onto the sensor plane. The transducer was driven by a pulse or a variable length toneburst, and the focus was moved manually across the sensor plane. Measurements were made in two different modes: in the first, the data was recorded at a rate limited by the DMD pattern refresh rate (or the ultrasound pulser if slower), and the reconstructions were postprocessed *offline* using the sparse nonlinear reconstruction described in Supplement 1. To demonstrate a real-time capability, a second mode, in which the reconstruction was performed *on-the-fly* between frames as soon as the data was measured, allowed *real-time* visualization of the acoustic field, albeit at a slower frame rate than could be achieved in the *offline* approach. In this case, the reconstruction used a zero-padded fast Hadamard transform (see Supplement 1).

Figure 3 and Visualization 1 and Visualization 2 demonstrate that a moving ultrasound field can be imaged using a pattern-based optical detection scheme suitable for CS. The main image in Fig. 3 shows the unprocessed time series data recorded in *offline* mode as the transducer focus was moved laterally across the sensor. Some vertical motion accompanied the lateral motion, as can be seen in the variation in time-of-arrival of the signal. This data was divided into subsets of 128 time series (compression 12.5%) and reconstructed into 3D (x, y, t) frames using the nonlinear

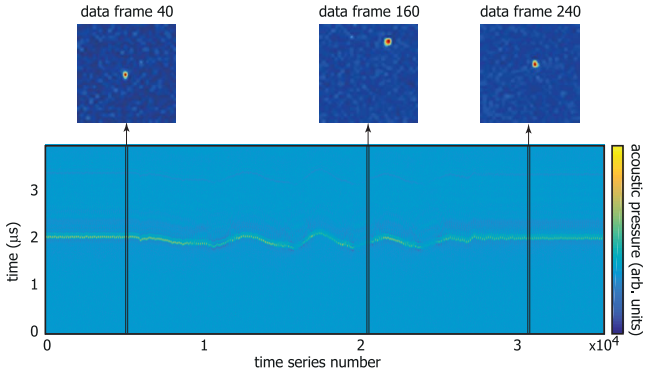

Fig. 3. Mapping the field of a moving focused ultrasound transducer (39 fps). The main figure shows 35,584 time series (278 consecutive data frames of 128 time series each) recorded while the ultrasound transducer focus was moved across the plane of the sensor. The data was recorded in *offline* mode with a pattern refresh rate of 5 kHz (limited by the transducer pulse repetition rate). For a $32 \times 32 = 1024$ pixel image, compression of 12.5% achieved a frame rate of 39 fps. Each reconstructed frame consists of a 3D dataset of the time evolution of the acoustic field at the sensor as the ultrasound pulse passes through it. The smaller figures above show MIPs over time, over the 4 μs of the measurement, for reconstructed frames 40, 160, and 240. See also Visualization 1 and Visualization 2.

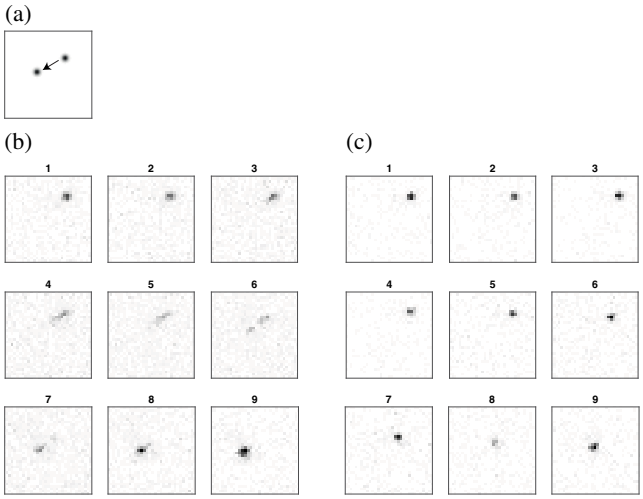

Fig. 4. Reducing motion blur in ultrasound field mapping by using CS. The ultrasound transducer focus was moved across the sensor while the data was recorded in *offline* mode (pattern refresh rate 2.5 kHz). (a) Schematic of the motion of the focus. (b) Nine frames at 102 ms intervals (10 fps)—the time required to record 256 patterns—reconstructed using 1024 patterns, so each time series was used in four consecutive frames. (c) The same data also reconstructed into nine frames spaced at 102 ms, but using CS with 256 patterns per frame, so no data is shared between consecutive frames. CS reduces the motion blur, clearly visible in (b), frames 4–7, but no longer visible in (c). The nonlinear reconstruction (see Supplement 1) restored the contrast and reduced the background noise. The differences between the reconstructions are best seen in Visualization 3, which shows these frames in a movie as part of a longer series.

reconstruction described in Supplement 1, giving a frame rate of 39 frames per second (fps).

The maximum intensity projections (MIPs), projections along the time axes, are also shown in the figure for three frames corresponding to different transducer positions. Visualization 1 and Visualization 2 show the ultrasound field in a similar scenario but recorded in real time using *on-the-fly* mode, first with no compression (Visualization 1) and then using just 12.5% of the full sets of patterns per frame (Visualization 2). Each frame of Visualization 1 (no compression) requires 8 times as long to acquire the data as Visualization 2 (12.5% compression), hence the motion in Visualization 2 appears more fluent. The loss of contrast—increase in background noise level—is due to the non-optimal Hadamard reconstruction used here because it is fast. These Visualizations illustrate well the real-time dynamic nature of the measurements.

The examples shown in Figs. 4 and 5 and Visualization 3 and Visualization 4 demonstrate two advantages of the increased frame rate that can be achieved through the use of CS. To obtain the data for Fig. 4 and Visualization 3, the moving ultrasound focus was imaged using a full set of 1024 patterns arranged in a random order and then cycled through repetitively in that order as long as required. Because of this arrangement, any consecutive set of 1024 patterns constituted a full set and could be used to reconstruct a frame without compression. Figure 4(a) is a schematic indicating the motion of the ultrasound focus during the nine frames shown in Figs. 4(b) and 4(c). Each frame in Fig. 4(b) was obtained using 1024 time series, but as frames were reconstructed for every 102 ms (10 fps)—time for just 256 time series to be recorded—each frame overlapped subsequent frames by 768 time series; each time series was used in four consecutive frames. The motion blur due to this sharing of time series between frames is evident, but can be removed using CS. Figure 4(c) was obtained using 256 time series per frame, compressed to 25%, so each frame is independent of its neighbors and the motion blur is absent. Visualization 3, which consists of a longer series of frames from which the nine frames in Figs. 4(b) and 4(c) were taken, shows the effect even more clearly than the static images.

For the example in Fig. 5 and Visualization 4, the ultrasound transducer was driven with a toneburst whose duration was varied cyclically from 2 periods to 3, 4, 5, then back to 2, etc. The changes were made at a rate of 50 Hz. The unprocessed time series data is shown in Fig. 5(d) and one reconstructed frame is shown in the maximum intensity projections, Figs. 5(a)–5(c). As with the previous example, the frames were reconstructed in two ways for comparison: Fig. 5(e) shows reconstruction without CS, so using overlapping 100% pattern sets, and Fig. 5(f) shows reconstruction with compression to 25%. The temporal variations in the toneburst that can be clearly seen in the raw data in Fig. 5(d) are averaged out in Fig. 5(e) when CS is not used, but are clearly evident when CS is employed as illustrated in Fig. 5(f).

In summary, it has been shown that by encoding an ultrasonic field onto an optical field and employing compressed sensing techniques it is possible to image broadband ultrasound fields in 2D at video frame rates of up to 78 fps with a single optical detector. As the aim of this study was to demonstrate the principle of this novel optical approach to ultrasonic measurement, the sensitivity and resolution were not optimized. However, just as in the case of a single-point scanner [15], there is considerable scope to increase the sensitivity by optimizing the interrogation laser intensity and the properties of the FP sensor (finesse, spacer thickness, and material properties).

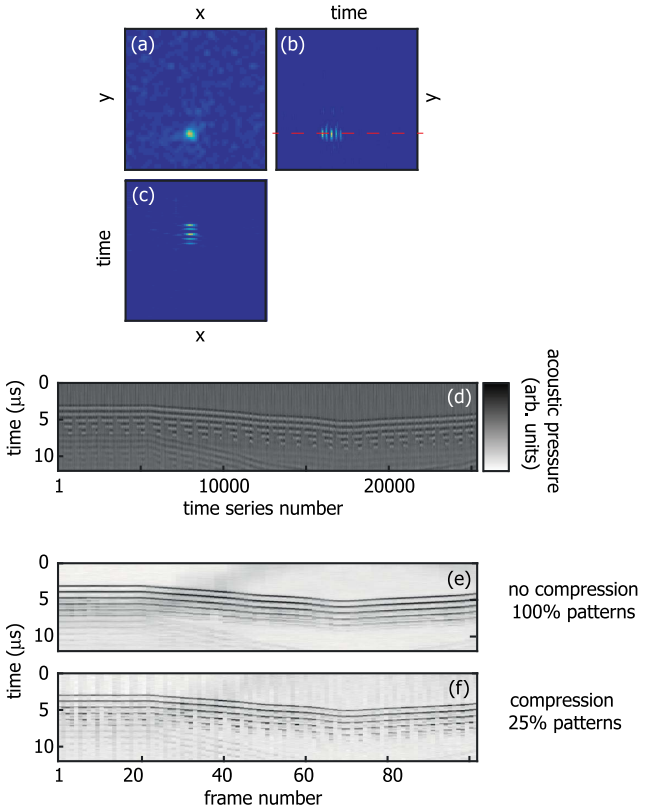

Fig. 5. Ultrasound field mapping with improved temporal resolution using CS (78 fps). The ultrasound field was recorded while the number of periods in the toneburst was cyclically varied (2,3,4,5,2, etc.) at a rate of 50 Hz. (1024 patterns, refresh rate 20 kHz limited by the DMD, *offline* mode). (a)–(c) One frame, showing maximum intensity projections along different axes: (a) time, (b) x, and (c) y. (d) The unprocessed time series measurements, showing the temporal variation in the toneburst. (e) and (f) Time profiles for the pixels of maximum intensity for each frame [dashed line through (b)]. (e) No compression: 1024 patterns per frame, overlapped such that each pattern contributes to four frames. Nominal frame rate 78 fps. (f) Compression 25%: 256 patterns per frame with no overlapping, giving a genuine 78 independent frames per second. The improved time resolution due to CS is evident here, but is best viewed in Visualization 4.

In the examples shown here, the resolution was limited by the low pixel count. Increasing the pixel count would require more patterns for the same compression rate. However, it is expected that using more pixels would allow higher compression rates for the same image quality.

This proof-of-principle study shows that this new approach to real-time ultrasound imaging offers a solution to the prohibitively high cost and technical complexity of conventional fixed element arrays, such as those based on piezoelectric receivers. As such, it could pave the way to realizing dynamic 3D photoacoustic and ultrasound imaging with broad application in medicine, biology, materials characterization, and metrology.

Funding. Engineering and Physical Sciences Research Council (EPSRC) (EP/K009745/1); European Research Council (ERC) (FP7-ICT (FAMOS, Contract 317744)).

See Supplement 1 for supporting content.

REFERENCES

1. M. F. Duarte, M. A. Davenport, D. Takhar, J. N. Laska, T. Sun, K. F. Kelly, and R. G. Baraniuk, IEEE Signal Process. Mag. **25**(2), 83 (2008).
2. K. Goda, K. K. Tsia, and B. Jalali, Nature **458**, 1145 (2009).
3. Y. Zhao, Z. Stratton, F. Guo, M. Lapsley, C. Chan, S. Lin, and T. Huang, Lab Chip **13**, 17 (2013).
4. P. Beard, Interface Focus **1**, 602 (2011).
5. K. K. Shung, J. Med. Ultrasound **17**, 25 (2009).
6. A. Arca, J. Aylott, L. Marques, M. Clark, M. Somekh, R. Smith, S. Sharples, T. Stratoudaki, and X. Chen, Nondestr. Test. Eval. **26**, 353 (2011).
7. B. E. Treeby, E. Z. Zhang, A. S. Thomas, and B. T. Cox, Ultrasound Med. Biol. **37**, 289 (2011).
8. B. Zeqiri, W. Scholl, and S. P. Robinson, Metrologia **47**, S156 (2010).
9. S. Umchid, R. Gopinath, K. Srinivasan, P. Lewin, A. Daryoush, L. Bansal, and M. El-Sherif, Ultrasonics **49**, 306 (2009).
10. B. Zeqiri, Prog. Biophys. Molec. Biol. **93**, 138 (2007).
11. M. Klann and C. Koch, IEEE Trans. Ultrason. Ferroelectr. Freq. Control **52**, 1546 (2005).
12. M. Lustig, D. Donoho, and J. M. Pauly, Magn. Reson. Med. **58**, 1182 (2007).
13. Y. Hou, J.-S. Kim, S. Ashkenazi, S.-W. Huang, L. J. Guo, and M. O'Donnell, Appl. Phys. Lett. **91**, 073507 (2007).
14. P. Hajireza, K. Krause, M. Brett, and R. Zemp, Opt. Express **21**, 6391 (2013).
15. E. Zhang and P. Beard, IEEE Trans. Ultrason. Ferroelectr. Freq. Control **53**, 1330 (2006).
16. S. Ashkenazi, R. Witte, and M. O'Donnell, Proc. SPIE **5697**, 243 (2005).
17. J. D. Hamilton, T. Buma, M. Spisar, and M. O'Donnell, IEEE Trans. Ultrason. Ferroelectr. Freq. Control **47**, 160 (2000).
18. B. Cong, K. Kondo, M. Yamakawa, T. Shiina, T. Nakajima, and Y. Asao, IEEJ Trans. Electr. Electron. Eng. **9**, 477 (2014).
19. R. Nuster, P. Slezak, and G. Paltauf, Biomed. Opt. Express **5**, 2635 (2014).
20. Y. Shu, X. Guo, M. Liu, and T. Buma, in *Proceedings of Ultrasonics Symposium* (IEEE, 2010), pp. 2396–2399.
21. M. Lamont and P. Beard, Electron. Lett. **42**, 187 (2006).
22. E. Zhang, J. Laufer, and P. Beard, Appl. Opt. **47**, 561 (2008).
23. R. G. Baraniuk, IEEE Signal Process. Mag. **24**(4), 118 (2007).
24. E. J. Candes, J. K. Romberg, and T. Tao, Commun. Pure Appl. Math. **59**, 1207 (2006).
25. M. Fornasier and H. Rauhut, in *Handbook of Mathematical Supplementary Material in Imaging* (Springer, 2011), pp. 187–228.
26. L. Gan, T. T. Do, and T. D. Tran, "Fast compressive imaging using scrambled block Hadamard ensemble," *Proceedings of European Signal Processing Conference*, Switzerland, 2008.